Chinese Chemical Letters 36 (2025) 109840

Contents lists available at ScienceDirect

Chinese Chemical Letters

journal homepage: www.elsevier.com/locate/cclet

A dual drug-loaded tumor vasculature-targeting liposome for tumor vasculature disruption and hypoxia-enhanced chemotherapy

Cheng-Zhe Gao, Hao-Ran Jia, Tian-Yu Wang, Xiao-Yu Zhu, Xiaofeng Han, Fu-Gen Wu*

State Key Laboratory of Digital Medical Engineering, Jiangsu Key Laboratory for Biomaterials and Devices, School of Biological Science and Medical Engineering, Southeast University, Nanjing 211189, China

ARTICLE INFO

Article history:
Received 24 January 2024
Revised 25 March 2024
Accepted 27 March 2024
Available online 28 March 2024

Keywords:
Tumor-homing peptide
Liposome
Vascular disrupting agents
Chemotherapy
Hypoxia-activated

ABSTRACT

Vascular disrupting agents (VDAs) can destroy tumor vasculature and lead to tumor ischemia and hypoxia, resulting in tumor necrosis. However, VDAs are easy to induce the upregulation of genes that are associated with cancer cell drug resistance and angiogenesis in tumor cells. Hypoxia-activated chemotherapy will be an ideal supplement to VDAs therapy since it can help to fully utilize the ischemia and hypoxia induced by VDAs to realize a synergistic antitumor therapeutic outcome. Here, we design a liposome whose surface is modified with a tumor-homing peptide Cys-Arg-Glu-Lys-Ala (CREKA, which can specifically target tumor vessels and stroma) and whose aqueous cavity and lipid bilayer are loaded by a hypoxia-activatable drug banoxantrone dihydrochloride (AQ4N) and a VDA combretastatin A4 (CA4), respectively. CA4 can selectively target vascular endothelial cells and destroy the tumor blood vessels, which will cause the rapid inhibition of blood flow in tumor and enhance the hypoxia in the tumor region. As a consequence, AQ4N can exert its boosted cytotoxicity under the enhanced hypoxic environment. The as-prepared liposome with a uniform particle size exhibits good stability and high cancer cell killing efficacy *in vitro*. In addition, *in vivo* experiments confirm the excellent tumor-targeting/accumulation, tumor vasculature-damaging, and tumor inhibition effects of the liposome. This work develops a liposomal which can achieve safe and effective tumor suppression without external stimulus excitation by only single injection, and is expected to benefit the future development of effective antitumor liposomal drugs.

Cancer is a major hazard to human health, and the attempts to treat it can be traced back to thousands of years ago [1]. However, most antitumor drugs destroy cancer cells as well as healthy tissues, and the lack of tumor selectivity of these drugs becomes the main factor limiting their safe and effective application [2]. Therefore, how to deliver antitumor drugs into the tumor area and minimize the side effects of the drugs has become a critical issue in cancer treatment [3]. Liposome, one of the most important nanoscale drug carriers, has a wide range of applications in antitumor drug delivery [4]. The hydrophobic lipid tail region and the inner aqueous cavity of a liposome enable it to carry various antitumor drugs to achieve diverse tumor therapies, such as chemotherapy [5], photodynamic therapy (PDT) [6,7], photothermal therapy [8,9] and immunotherapy [10,11]. Compared with the relevant free drugs, the drugs encapsulated in liposomes can significantly avoid the off-target cytotoxicity and reduce the side effects in tumor therapy [12]. This is because the nanoscale liposomes cannot easily penetrate into normal tissues with tight endothelial junctions, but they can passively accumulate in tumor areas with higher vascular permeability. Moreover, the surface groups of some liposomes can be conjugated with functional ligands conveniently [13]. So far, many biomolecules have been used as targeting ligands for the modification of liposomes [14–21]. Cys-Arg-Glu-Lys-Ala (CREKA) is a short linear peptide that can recognize and selectively target tumor by binding to the highly expressed fibronectin in the tumor vessel wall and stroma [5,22]. Owing to its tumor-targeting ability, CREKA has shown outstanding potential in tumor treatment and has been applied in many antitumor studies [23–28].

Hypoxia is a main characteristic of tumor microenvironment and a high-priority therapeutic target [29]. The strategies for hypoxia-enhanced and hypoxia-activated tumor therapy have been frequently reported in the last few years [30–36]. Some hypoxia-activatable drugs, such as banoxantrone dihydrochloride (AQ4N), can be reduced from nontoxic prodrugs to toxic drugs under a hypoxic condition [37], which means that they can precisely target hypoxic tumor cells and have little toxicity to normal tissue [38]. The hypoxia activation of drugs makes hypoxia not a problem

* Corresponding author.
E-mail address: wufg@seu.edu.cn (F.-G. Wu).

https://doi.org/10.1016/j.cclet.2024.109840
1001-8417/

promoting tumor progress but an advantage enabling selective anticancer treatment [39]. However, inadequate hypoxia within the tumor during therapy has become an obstacle of some hypoxia-activated prodrugs in clinical trials [40].

Vascular occlusion is an efficacious way to enhance the level of hypoxia. Besides enhancing hypoxia, it can also inhibit the tumor aggressiveness by inhibiting angiogenesis [41,42]. Vascular disrupting agents (VDAs), a kind of tumor therapy drugs, can selectively target and destroy tumor vasculature, which will lead to rapid inhibition of blood flow in tumors and cause tumor ischemia and hypoxia, resulting in tumor necrosis [43,44]. Combretastatin A4 (CA4) is a small-molecule VDA extracted from the African tree *Combretum caffrum* [45], which can destroy the cytoskeleton of tumor vascular endothelial cells, thereby leading to the collapse of blood vessels and further resulting in the ischemia-induced tumor cell death [41,44]. Meanwhile, the blood blockage induced by CA4 can significantly reduce the oxygenation of tumor and cause hypoxia [46]. The common strategies that can enhance hypoxia by oxygen consumption include PDT and sonodynamic therapy (SDT). However, they usually have inherent shortages. For example, PDT is often restricted by the low optical penetration depth, while SDT is limited by the self-quenching effect caused by the aggregation of high-concentration sonosensitizers. Compared with them, vascular disruption can stably induce tumor hypoxia without the activation of external stimuli, which makes vascular disruption more suitable for systemic therapy.

However, the hypoxic environment caused by VDAs can upregulate the genes associated with angiogenesis [47], which makes the survived tumor cells adapt to the hypoxic environment better and develop the drug resistance to VDAs, thereby seriously limiting the application of VDAs [48]. On the other hand, the ischemia and hypoxia in the tumor caused by VDAs have not been fully utilized in many previous studies, which largely impairs VDAs' cancer treatment efficacy. Therefore, hypoxia-activatable chemodrugs, such as AQ4N, will be an ideal supplement since they can help to kill tumor cells effectively under the elevated hypoxia condition and avoid the risk of tumor recurrence resulting from hypoxia adaptation. However, the investigation of nanosystems integrating these two types of drugs (VDA and hypoxia-activatable chemodrug) is still inadequate, even if the potential synergy was often mentioned in some previous researches [40,49,50]. Meanwhile, although there are several clinical trials that use liposomes as the carriers to encapsulate chemotherapeutic drugs, most of the liposomes still have similar features with those already clinically approved, like poly(ethylene glycol) (PEG) modification, nontargetable property, and single-drug loading [51,52]. Consequently, designing a targetable and multidrug-loaded liposome without the requirement of external stimulus activation for efficient tumor combination therapy is highly desired but still remains a challenge.

In this work, we designed a targeting liposome (TL) (termed CA-TL) modified with the tumor-homing peptide CREKA and loaded with the VDA CA4 and the hypoxia-activatable chemotherapeutic drug AQ4N. The encapsulation *via* liposomes overcomes the poor water-solubility of CA4. CREKA endows the liposomal nanodrug with excellent tumor targeting capacity. CA4 and AQ4N could enhance hypoxia and induce responsive cytotoxicity, respectively. The disruption of tumor vessels by CA4 can enhance hypoxia in the tumor area. And under the enhanced hypoxic condition, AQ4N will be converted to cytotoxic AQ4, thereby killing tumor cells (Scheme 1). Impressively, CA-TL can achieve safe and effective tumor suppression without external stimulus excitation by only single injection. The therapeutic results indicated that the CA-TL had a high tumor inhibitory efficacy with marginal side effect.

To link the CREKA peptide on the surface of the liposome, we synthesized a CREKA-conjugated PEG-lipid (DSPE-PEG_{2000}-CREKA) by the reaction between the thiol group-containing CK-

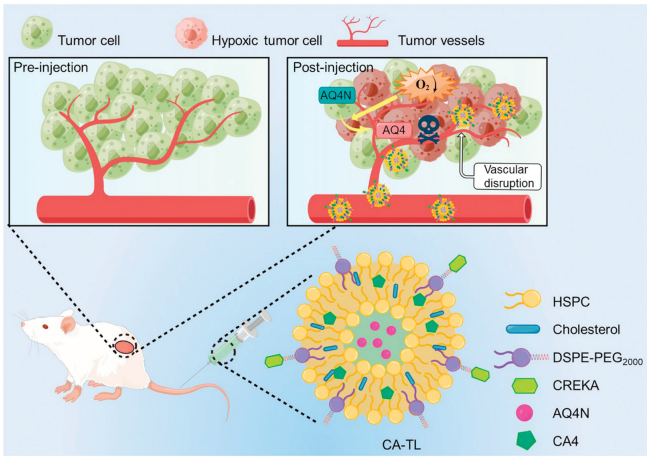

Scheme 1. Scheme showing the chemical composition of CA-TL and the hypoxia-activated cancer therapy induced by CA-TL.

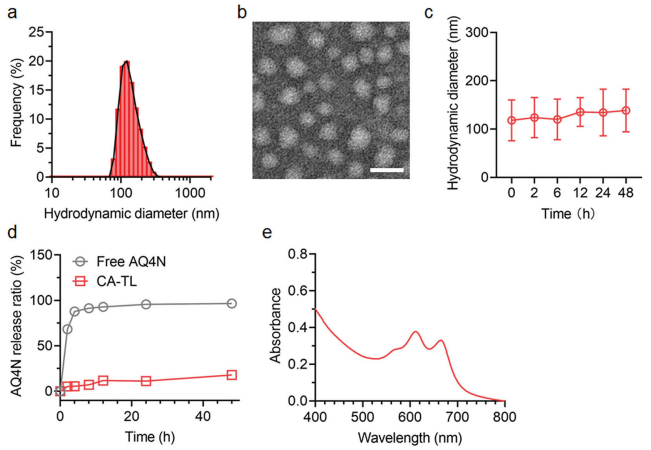

Fig. 1. (a) Hydrodynamic diameter and (b) TEM image of CA-TL. Scale bar: 100 nm. (c) Changes in the hydrodynamic diameter of CA-TL (in PBS) within 48 h. (d) Drug (AQ4N) release profiles of free AQ4N and CA-TL in PBS (pH 7.4) at room temperature. (e) UV–vis absorption spectrum of CA-TL dispersed in PBS. The statistical data were expressed as mean ± standard deviation (SD) ($n = 3$).

REA and the maleimide group-containing 1,2-distearoyl-*sn*-glycero-3-phosphoethanolamine-*N*-[maleimide(polyethylene glycol)-2000] (DSPE-PEG_{2000}-Mal). Mass spectrometry was used to prove the successful synthesis of DSPE-PEG_{2000}-CREKA. The results in Figs. S1a and b (Supporting information) showed that the mass-to-charge ratio peak increased from 2930.5 (DSPE-PEG_{2000}-Mal) to 3531.3 (DSPE-PEG_{2000}-CREKA), and the molecular weight increase of ~601 was close to the molecular weight of CREKA, demonstrating the successful conjugation of the peptide to the PEG-lipid. The CA-TL and other liposomes (liposomes without CREKA, termed CA-L; CREKA-conjugated liposomes only loaded with AQ4N, termed A-TL; CREKA-conjugated liposomes only loaded with CA4, termed C-TL; liposomes without CREKA and only loaded with AQ4N, termed A-L) were further synthesized according to the procedures described in the supporting information. As revealed by dynamic light scattering (DLS), the hydrodynamic diameter of CA-TL was 123 ± 41 nm (Fig. 1a). The zeta potential of CA-TL was measured to be −16.6 ± 0.5 mV (Fig. S2 in Supporting information). Besides, the hydrodynamic diameters and zeta potentials of other liposomes (A-L, A-TL, C-TL, and CA-L) were also measured, and the corresponding results were shown in Table S1 and Fig. S2 (Supporting information). In addition, the transmission electron microscopy (TEM) image in Fig. 1b and the corresponding statistical result in Fig.

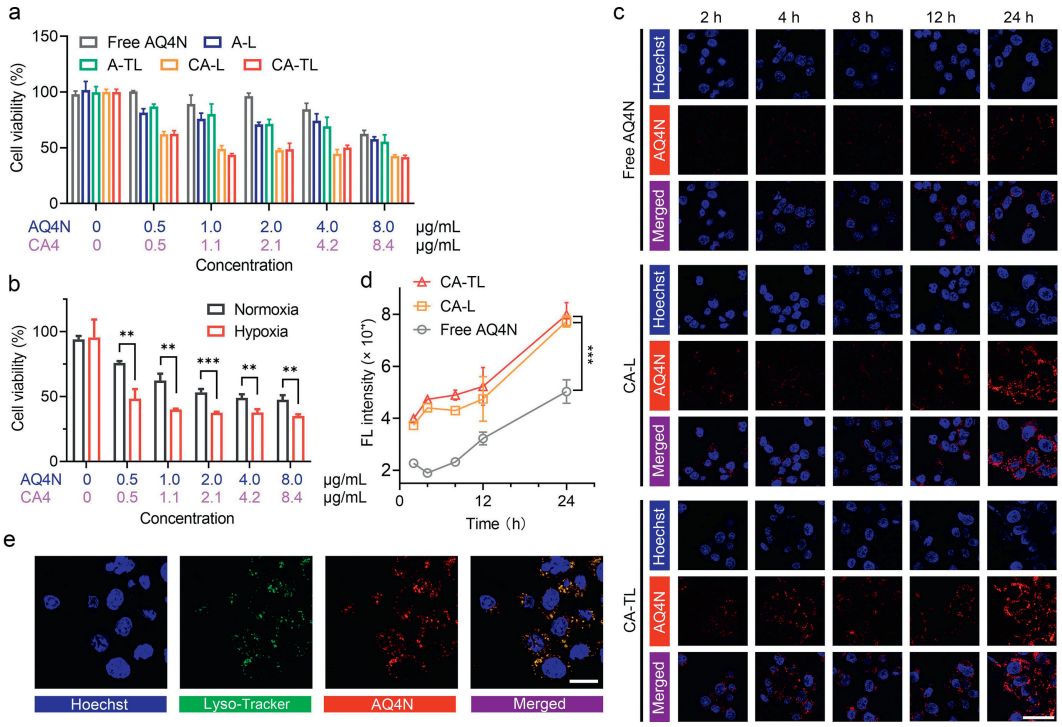

Fig. 2. (a) Relative viabilities of 4T1 cells after incubation with free AQ4N, A-L, A-TL, CA-L, or CA-TL. (b) Relative viabilities of 4T1 cells after incubation with CA-TL under the normoxia or hypoxia culture condition. (c) Confocal fluorescence images of 4T1 cells after being treated with free AQ4N, CA-L, or CA-TL (the concentration of AQ4N in each sample was 4 μg/mL) for 2, 4, 8, 12, and 24 h. Before imaging, the treated cells were stained by the nuclear dye Hoechst 33342 (abbreviated as Hoechst in the figure). Scale bar: 40 μm. (d) Flow cytometric results of 4T1 cells incubated with CA-TL, CA-L or free AQ4N (the concentration of AQ4N in each sample was 4 μg/mL) for different time periods. (e) Confocal fluorescence images of 4T1 cells. Before imaging, the cells were treated with CA-TL (the concentration of AQ4N in the sample was 4 μg/mL) for 4 h, and stained by Hoechst 33342 and the lysosomal dye Lyso-Tracker Green (abbreviated as Lyso-Tracker in the figure). Scale bar: 20 μm. $^{**}P < 0.01$, $^{***}P < 0.001$. The statistical data were expressed as mean ± SD ($n = 3$).

S3 (Supporting information) showed that the CA-TL were spherical particles with an average size of 50.3 ± 8.6 nm. To check the stability of liposomes, DLS was adopted to monitor the changes in the hydrodynamic diameter of CA-TL within 48 h. The results in Fig. 1c revealed that the diameter of CA-TL did not have significant changes, confirming the good colloidal stability of the liposomes. Moreover, as shown in Fig. 1d, the drug (AQ4N) release profiles of free AQ4N and CA-TL indicated that AQ4N could be stably loaded by the liposomes. To quantify the encapsulation efficiency and loading capacity of the drugs, we measured the ultraviolet–visible (UV–vis) absorption spectra of CA-TL in phosphate-buffered saline (PBS) (Fig. 1e) and in dimethyl sulfoxide (DMSO) (Fig. S4a in Supporting information), respectively. In addition, the absorption spectra of different concentrations of AQ4N (dispersed in PBS) and CA4 (dispersed in DMSO) standard samples (Figs. S4b and c in Supporting information) were also measured for linear fitting of the standard curves, and the concentrations of AQ4N and CA4 in CA-TL were determined by their absorption values through the standard curves (Figs. S4d and e in Supporting information). The encapsulation efficiencies and drug loading capacities of AQ4N (or CA4) were determined by the equations listed in the supporting information and displayed in Table S2 (Supporting information).

Next, the cytotoxicity and cellular uptake of liposome were explored, we found that compared with free AQ4N and A-TL, the liposomal nanodrugs containing CA4 (CA-L and CA-TL) were more cytotoxic to the 4T1 murine mammary carcinoma cells under normoxic conditions (Fig. 2a). However, free AQ4N, A-L, and A-TL did not show significant cytotoxicity at low concentrations because of the normoxic condition *in vitro*. AQ4N is expected to become more cytotoxic under the hypoxic condition of a tumor *in vivo*. Further experimental results in Fig. 2b and Fig. S5 (Supporting information) proved that the cytotoxicities *via* free AQ4N, A-TL, and CA-TL were significantly enhanced under hypoxia, and the increase of cytotoxicity was attributed to the reduction of AQ4N. Then, the cellular uptake of AQ4N over time was observed by confocal microscopy. The images in Fig. 2c demonstrated that free AQ4N gradually accumulated in 4T1 cells within 12 h, and CA-TL exhibited increased cellular uptake of AQ4N relative to free AQ4N. The results of fluorescence quantification (Fig. S6 in Supporting information) and flow cytometry (Fig. 2d) also reached a similar conclusion that the cellular uptake of CA-TL was increased compared with free AQ4N. The conclusion indicated that the encapsulation *via* liposome could increase the cellular uptake of AQ4N. Next, we evaluated the cellular localization of CA-TL. The confocal microscopic images in Fig. 2e showed that the AQ4N molecules were colocalized with lysosomes, which proved that the AQ4N molecules were captured by lysosomes in cells after the liposomes loaded with AQ4N entered the cells.

Moreover, the endocytosis pathways of CA-TL and CA-L in 4T1 cells were investigated. The inhibitor of micropinocytosis (5-(*N*,*N*-dimethyl)amiloride hydrochloride, abbreviated as amiloride), the inhibitor of lipid raft-mediated endocytosis (methyl-β-cyclodextrin, abbreviated as MβCD), the inhibitor of caveolae-mediated endocytosis (genistein), and the inhibitor of clathrin-mediated endocytosis (chlorpromazine hydrochloride, abbreviated as CPZ) were used to inhibit the corresponding endocytosis pathways. Besides, to investigate if the cellular uptake of CA-TL and CA-L was energy-dependent, 4 °C treatment was also applied in the experiment. The flow cytometric assay results were shown in Fig. S7 (Supporting information). Compared with the control group, the CA-TL endocytosis ratios of amiloride, MβCD, genistein, and CPZ groups decreased by around 14.1%, 25.7%, 4.8%, and 5.8%, re-

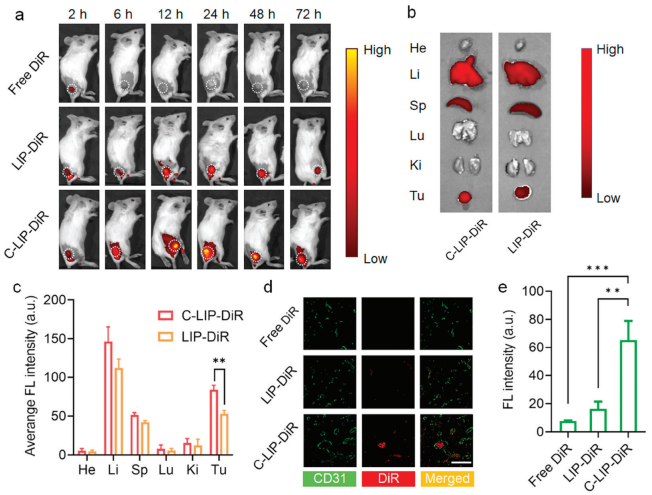

Fig. 3. (a) *In vivo* fluorescence images of mice treated with free DiR, LIP-DiR, or C-LIP-DiR (200 μg DiR/kg mouse) at 2, 6, 12, 24, 48, and 72 h post injection. (b) *Ex vivo* fluorescence images of the main organs and tumor tissues that were collected from the mice at 72 h post the injection of C-LIP-DiR or LIP-DiR. He, Li, Sp, Lu, Ki, and Tu stand for heart, liver, spleen, lung, kidneys, and tumor, respectively. (c) Corresponding quantitative fluorescence analysis results of each organ in (b). (d) Immunofluorescence staining results of tumor tissue slices from the mice treated with free DiR, LIP-DiR, or C-LIP-DiR for 72 h. Scale bar: 100 μm. (e) Corresponding fluorescence intensities of DiR in (d). $^{**}P < 0.01$, $^{***}P < 0.001$. The statistical data were expressed as mean ± SD ($n = 3$).

spectively, which could verify that the endocytosis of CA-TL mainly depends on lipid raft-mediated endocytosis and micropinocytosis. Meanwhile, it was noticed that 4 °C treatment reduced the endocytosis ratio of CA-TL by over 90%, which confirmed that the endocytosis of CA-TL was energy-dependent. The endocytosis performance of the CA-L group had no significant difference with that of the CA-TL group, implying that the CREKA modification did not affect the endocytosis pathway of the liposome.

As a kind of microtubule-binding drug, CA4 can bind to the microtubules of vascular endothelial cells and cause the depolymerization and instability of cytoskeleton [53]. To investigate this effect of CA4 toward vascular endothelial cells, we treated human microvascular endothelial cells (HMECs) with free CA4 or C-TL. The images in Fig. S8 (Supporting information) showed that the shape of HMECs was significantly changed, which indicated that the structure of the treated HMECs was seriously disrupted by free CA4 or C-TL. Specifically, after CA4 treatment, some cells became spherical in shape, while the untreated HMECs were fusiform. The change of cell morphology might be caused by the loss of supporting after the destruction of cytoskeleton in cells. The additional results in Fig. S9 (Supporting information) further indicated that CA4 could induce structural destruction of the cytoskeleton in HMECs. Hence, using HMECs as the example, we proved that CA4 could disrupt the structure of vascular endothelial cells by destroying the cytokeleton. In solid tumors, the above effect may lead to the collapse of tumor vessels, thus inducing the enhanced hypoxia.

To investigate the targeting effect of CREKA *in vivo*, we prepared empty DiR-labeled liposomes with or without CREKA modification (C-LIP-DiR and LIP-DiR). The *in vivo* biodistribution analysis was carried out on 4T1 tumor-bearing mice. All the experimental procedures regarding animals in this work were performed under the approval of the Animal Care & Welfare Committee of Southeast University (approval number: 20220907001) and conducted in compliance with the Regulations for the Administration of Affairs Concerning Experimental Animals of China. Fluorescence imaging was performed on tumor-bearing mice at different time points after injection. As shown in the *in vivo* fluorescence images (Fig. 3a), at each time point, the C-LIP-DiR group was found to show the strongest fluorescence in the tumor region. Besides, because of the high stability of the binding between CREKA and the fibronectin, the liposomes modified with CREKA could retain in the tumor area for a much longer time period. Specifically, the C-LIP-DiR group still maintained a strong fluorescence signal at 72 h after injection, demonstrating that the modification of CREKA enhanced the enrichment and retention of the liposomal nanodrug in the tumor region. At 72 h post injection, the distribution patterns of C-LIP-DiR and LIP-DiR in the major organs were examined *via ex vivo* fluorescence imaging. The results in Figs. 3b and c also demonstrated that the fluorescence of the tumor in the C-LIP-DiR group was significantly stronger than that in the LIP-DiR group. In other organs except tumor, the two liposomes exhibited a similar degree of accumulation, which indicated that there was no obvious difference between the two liposomes in systemic clearance.

As displayed in the immunofluorescence staining results (Fig. 3d), we could see that red fluorescence signals accumulated at the tumor areas with abundant blood vessels in the C-LIP-DiR group, and some of the blood vessels appeared to have their lumens filled with evident red fluorescence signals (from DiR), which could not be observed in the other two groups. This result indicated that C-LIP-DiR might accumulate in tumor blood vessels, while LIP-DiR, the liposome without CREKA modification, did not exhibit the same ability. The corresponding fluorescence intensity results (Fig. 3e) verified that the red fluorescence intensity from the DiR of the C-LIP-DiR group was much higher than that of the other two groups. The above results suggested that the C-LIP-DiR has an enhanced tumor-targeting effect.

In vivo antitumor experiments were carried out on 4T1 tumor-bearing mice. The photographs of the tumors in Fig. 4a showed that the CA-TL group had a better therapeutic effect than the other groups, indicating that the combined treatment of CA4 and AQ4N was highly beneficial for the antitumor efficacy, and the CREKA modification could also significantly strengthen the antitumor effect. The tumor growth curves in Fig. 4b also demonstrated the excellent inhibition effect of CA-TL on tumor growth. The average tumor volume (measured on day 18) in the CA-TL group is 26.5% of that in the CA-L group, 26.2% of that in the C-TL group, and 16.1% of that in the control group, respectively, which proved that CA-TL had an enhanced tumor-targeting ability and overcame the problem of the limited cytotoxicity of the liposome only containing CA4 (C-TL). Meanwhile, we noticed that although a moderate therapeutic effect was achieved in the A-TL group, the average tumor volume (measured on day 18) in the A-TL group was still 1.9-fold higher than that in the CA-TL group, which indicated that the increased toxicity of AQ4N under the enhanced hypoxic condition induced by the vascular disruption of CA4 could improve the antitumor efficacy of CA-TL. During treatment, the body weights of all the mice were monitored, and there were no obvious changes in all the groups (Fig. 4c), which demonstrated the favorable biocompatibility of these drugs.

Further, we performed hematoxylin and eosin (H&E) staining and terminal deoxynucleotidyl transferase-mediated dUTP nick-end labeling (TUNEL) assay experiments. As shown in Fig. 4d, compared with other groups, the H&E staining results revealed that the tumor tissues of the CA-TL-treated mice became looser, and the TUNEL staining results and corresponding fluorescence quantitative analysis results (Fig. S10 in Supporting information) showed that there was a higher level of apoptosis in the tumor tissue of the CA-TL group. Meanwhile, the cell apoptosis in the C-TL group did not have an obvious increase compared with that in the control group, indicating that the liposome only containing the drug CA4 (C-TL) could not effectively induce apoptosis *in vivo*.

To further explore the vascular disruption and hypoxia in tumor after different treatments, immunofluorescence staining was car-

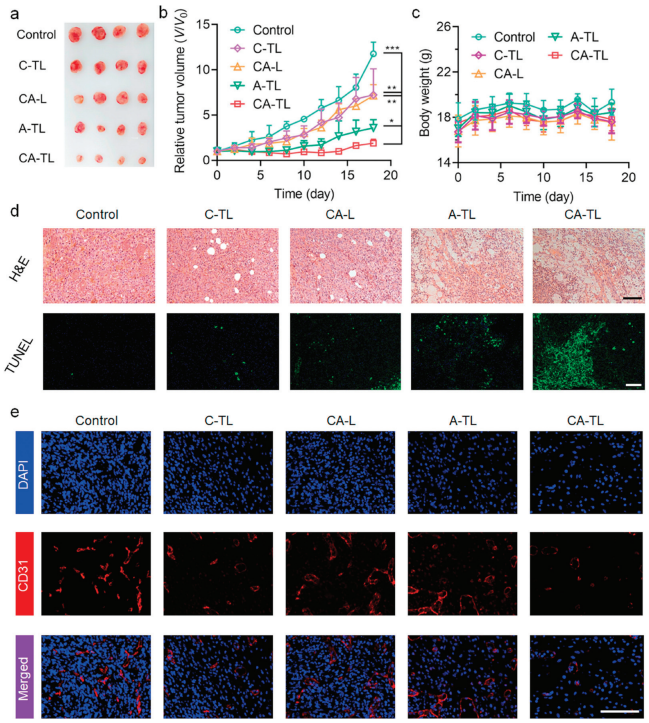

Fig. 4. Antitumor effects of different formulations in 4T1 tumor-bearing mouse models. (a) Representative photographs of the dissected tumors from various groups ($n = 4$). (b) Relative tumor volumes and (c) body weights of the tumor-bearing mice after different treatments. The statistical data were expressed as mean ± SD ($n = 4$). (d) H&E or TUNEL assay results of the tumor tissues from the tumor-bearing mice after various treatments. Scale bar: 100 μm. (e) Confocal fluorescence images of the immunofluorescence staining results of CD31 (reflecting tumor vessels) of the tumor tissue slices from the tumor-bearing mice after various treatments. Scale bar: 100 μm. The mice injected with PBS were set as the control group. $^{*}P < 0.05$, $^{**}P < 0.01$, $^{***}P < 0.001$.

ried out, and the corresponding results were shown in Fig. 4e and Fig. S11 (Supporting information). The amounts of tumor blood vessels in the C-TL and CA-TL groups were obviously smaller than those of other groups, which proved that CA4 caused serious damage to tumor blood vessels. The quantitative fluorescence results of CD31 shown in Fig. S12 (Supporting information) revealed that the CA-TL group had less CD31 than the C-TL group, which was due to the potentiated tumor eradication effect resulting from the enhanced cytotoxicity of AQ4N under hypoxia which could further inhibit the angiogenesis of tumor. Moreover, the levels of hypoxia-inducible factor 1α (HIF-1α) in the C-TL and CA-TL groups were also higher than those of the other three groups. Since the level of HIF-1α represents the hypoxia degree in tumor region, the above result indicated that the vascular disruption caused by CA4 could enhance the hypoxia of tumor. To sum up, the CA-TL performed better than the other groups in terms of the antitumor efficacy, which proved that AQ4N and CA4 had a good synergy in tumor treatment, and the modification of CREKA also enhanced the efficiency of tumor treatment.

Finally, the biosafety of CA-TL was evaluated. First, the blood from the mice 18 d after CA-TL injection was collected for blood routine and biochemical examinations. According to the results shown in Fig. S13 (Supporting information), there was no significant difference between the CA-TL-treated mice and the PBS-treated mice for all the blood indexes evaluated. The results indicated that the injection of CA-TL had no side effect to the mice. In addition, the H&E staining results of the main organs (Fig. S14 in Supporting information) demonstrated that there was no major organ damage after CA-TL treatment. The results above collectively indicated that CA-TL had good biosafety, confirming their potential for clinical applications.

In conclusion, we designed a new type of liposome termed CA-TL, which contained a tumor-homing peptide CREKA, a chemotherapeutic drug AQ4N, and a vascular disrupting agent CA4. CA-TL had the characteristics of uniform particle size and good *in vitro* stability. Compared with free AQ4N, the CA-TL had a higher tumor cell uptake and a better tumor cell killing effect. In addition, the *in vivo* fluorescence imaging results demonstrated that CREKA could largely enhance the tumor-targeting ability of CA-TL. *In vivo* tumor therapeutic experiments revealed that the vascular disruption by CA4 exacerbated the ischemia and hypoxia in the tumor area, which increased the toxicity of the hypoxia-responsive chemotherapeutic drug AQ4N. Meanwhile, the cytotoxicity against tumor cells of AQ4N could further suppress the angiogenesis of tumor. The synergy between CA4 and AQ4N mutually inhibited the growth and angiogenesis of tumors, and achieved enhanced antitumor combination therapy. Taken together, our work realized the targeted delivery of CA4 and AQ4N by the CREKA-modified liposome, which could enable the accurate destruction of tumor vessels, exacerbate the tumor hypoxia, and subsequently activate the hypoxic cytotoxicity of AQ4N, thus achieving a synergistic antitumor therapeutic effect. The combination therapy not only overcomes the shortcomings of VDAs when used as the only antitumor drugs, but also makes full use of the aggravated hypoxia induced by tumor vasculature-targeted therapy. This work develops a novel liposomal drug that can achieve safe and effective tumor suppression without external stimulus excitation by using only a single injection, which will shed new light on the development of effective tumor vasculature-targeting nanomedicines.

Declaration of competing interest

The authors declare that they have no known competing financial interests or personal relationships that could have appeared to influence the work reported in this paper.

CRediT authorship contribution statement

Cheng-Zhe Gao: Conceptualization, Investigation, Writing – original draft. **Hao-Ran Jia:** Investigation. **Tian-Yu Wang:** Investigation. **Xiao-Yu Zhu:** Investigation. **Xiaofeng Han:** Writing – review & editing. **Fu-Gen Wu:** Conceptualization, Funding acquisition, Investigation, Resources, Supervision, Writing – review & editing.

Acknowledgments

This work was supported by the Key Laboratory of Early Prevention and Treatment for Regional High Frequency Tumor (Guangxi Medical University), Ministry of Education (No. GKE-KF202305), the Guangxi Key Laboratory of Early Prevention and Treatment for Regional High Frequency Tumor, and the Natural Science Foundation of Jiangsu Province (No. BK20211510). We would also like to thank Figdraw (www.figdraw.com) for assisting us in drawing the Scheme 1.

Supplementary materials

Supplementary material associated with this article can be found, in the online version, at doi:10.1016/j.cclet.2024.109840.

References

[1] L. Falzone, S. Salomone, M. Libra, Front. Pharmacol. 9 (2018) 1300.
[2] H. Dong, L. Pang, H. Cong, Y. Shen, B. Yu, Drug Deliv. 26 (2019) 416–432.
[3] T.O.B. Olusanya, R.R.H. Ahmad, D.M. Ibegbu, J.R. Smith, A.A. Elkordy, Molecules 23 (2018) 907.

[4] M. Slingerland, H.J. Guchelaar, H. Gelderblom, Drug Discov. Today 17 (2012) 160–166.
[5] K. Jiang, X. Song, L. Yang, et al., J. Control. Release 271 (2018) 21–30.
[6] Y.X. Zhu, H.R. Jia, Q.Y. Duan, et al., ACS Appl. Mater. Interfaces 12 (2020) 36882–36894.
[7] G. Lu, X. Gao, H. Zhang, et al., Chin. Chem. Lett. 33 (2022) 1923–1926.
[8] G. Gao, Y.W. Jiang, Y. Guo, et al., Adv. Funct. Mater. 30 (2020) 1909391.
[9] W. Hu, Q. Qi, H. Hu, et al., Colloids Surf. A 634 (2022) 127921.
[10] S. Watanabe, E. Yuba, T. Akazawa, et al., Vaccine 40 (2022) 1448–1457.
[11] H. Hu, L. Yu, Z. Ding, et al., Chin. Chem. Lett. 34 (2023) 108592.
[12] G. Berry, M. Billingham, E. Alderman, et al., Ann. Oncol. 9 (1998) 711–716.
[13] Y. Li, H. Cong, S. Wang, B. Yu, Y. Shen, Biomater. Sci. 8 (2020) 6442–6468.
[14] P. Deshpande, A. Jhaveri, B. Pattni, S. Biswas, V. Torchilin, Drug Deliv. 25 (2018) 517–532.
[15] Z. Zhang, J. Yang, Q. Min, et al., Small 15 (2019) 1803703.
[16] A. Akhtar, L. Ghali, S.X. Wang, et al., Int. J. Mol. Sci. 20 (2019) 2156.
[17] C. Qi, D. Wang, X. Gong, et al., ACS Appl. Mater. Interfaces 13 (2021) 16019–16035.
[18] L. Lu, Y. Ding, Y. Zhang, et al., Int. J. Nanomed. 13 (2018) 1927–1944.
[19] Y. Zhang, M. Zhai, Z. Chen, et al., Drug Deliv. 24 (2017) 1045–1055.
[20] G. Kibria, H. Hatakeyama, N. Ohga, K. Hida, H. Harashima, J. Control. Release 153 (2011) 141–148.
[21] X. Liu, J. Jiang, Y. Ji, et al., Mol. Syst. Des. Eng. 2 (2017) 370–379.
[22] J. Zhao, B. Zhang, S. Shen, et al., J. Colloid Interface Sci. 450 (2015) 396–403.
[23] C. Wang, X. Wang, T. Zhong, et al., Int. J. Nanomed. 10 (2015) 2229–2248.
[24] Q. Shi, Y. Zhang, S. Liu, et al., Biochem. Pharmacol. 156 (2018) 501–510.
[25] M. Geranpayehvaghei, Q. Shi, B. Zhao, et al., Bioconjug. Chem. 30 (2019) 2349–2357.
[26] B. Zhao, H. Wang, S. Shen, et al., Biomaterials 79 (2016) 46–55.
[27] J. Chen, Z. Zhang, Y. Li, et al., J. Mater. Chem. B 10 (2022) 8193–8210.
[28] Z. Zhou, X. Wu, A. Kresak, M. Griswold, Z.R. Lu, Biomaterials 34 (2013) 7683–7693.
[29] R.M. Phillips, Cancer Chemother. Pharmacol. 77 (2016) 441–457.
[30] X. Zhang, X. Chen, H.Y. Wang, H.R. Jia, F.G. Wu, Adv. Ther. 2 (2019) 1800140.
[31] Y. Guo, H.R. Jia, X. Zhang, et al., Small 16 (2020) 2000897.
[32] Y.X. Zhu, H.R. Jia, Y. Guo, et al., Small 17 (2021) 2100753.
[33] R. Zhang, L. Feng, Z. Dong, et al., Biomaterials 162 (2018) 123–131.
[34] Y. Wang, W. Shang, M. Niu, J. Tian, K. Xu, Int. J. Nanomed. 14 (2019) 3705–3722.
[35] M. Liu, L. Wang, X. Zheng, S. Liu, Z. Xie, ACS Appl. Mater. Interfaces 10 (2018) 24638–24647.
[36] D.C. Yang, L.F. Wen, L. Du, et al., ACS Appl. Mater. Interfaces 14 (2022) 40546–40558.
[37] L.H. Patterson, S.R. McKeown, Br. J. Cancer 83 (2000) 1589–1593.
[38] Y. Li, L. Zhao, X.F. Li, Front. Oncol. 11 (2021) 700407.
[39] S. Luo, C. Liang Q. Zhang, P. Zhang, Chin. Chem. Lett. 34 (2023) 107666.
[40] S. Yang, Z. Tang, C. Hu, et al., Adv. Mater. 31 (2019) 1805955.
[41] E. Abma, S. Daminet, P. Smets, Y. Ni, H. de Rooster, Vet. Comp. Oncol. 1 (2015) 184–193.
[42] S.R. Menakuru, N.J. Brown, C.A. Staton, M.W.R. Reed, Br. J. Cancer 99 (2008) 1961–1966.
[43] V.L. Heath, R. Bicknell, Nat. Rev. Clin. Oncol. 6 (2009) 395–404.
[44] L. Liu, D. O'Kelly, R. Schuetze, et al., Molecules 26 (2021) 2551.
[45] E. Porcù, R. Bortolozzi, G. Basso, G. Viola, Future Med. Chem. 6 (2014) 1485–1498.
[46] S. Dey, S. Kumari, S.P. Kalainayakan, et al., Oncotarget 9 (2018) 4090–4101.
[47] G.M. Tozer, C. Kanthou, G. Lewis, et al., Br. J. Radiol. 81 (2008) S12–S20.
[48] D. Zhao, X. Huang, Z. Zhang, et al., Wiley Interdiscip. Rev.: Nanomed. Nanobiotechnol. 13 (2021) e1691.
[49] M.M. Cooney, W. van Heeckeren, S. Bhakta, J. Ortiz, S.C. Remick, Nat. Clin. Pract. Oncol. 3 (2006) 682–692.
[50] Y.J. Ho, T.C. Wang, C.H. Fan, C.K. Yeh, Drug Discov. Today 22 (2017) 1503–1515.
[51] A.C. Anselmo, S. Mitragotri, Bioeng. Transl. Med. 1 (2016) 10–29.
[52] A.C. Anselmo, S. Mitragotri, Bioeng. Transl. Med. 4 (2019) e10143.
[53] E.L. Schwartz, Clin. Cancer Res. 15 (2009) 2594–2601.